ISSN 1330-3651 (Print), ISSN 1848-6339 (Online) https://doi.org/10.17559/TV-20230425000565
Preliminary communication

Design of Pulse Forming Networks Triggered by High-Power Hydrogen Thyratron

Yong HAN, Tao ZHAO, Shi YAN, Guang WEN, Zhaoyu WU*

Abstract: Hydrogen thyratron is a switching device invented based on the phenomenon of gas discharge, and it is widely used in the field of high-power pulse technology. The design of Pulse Forming Network (PFN) triggered by hydrogen thyratron aims to control the switch of subsequent circuit, and shorten the gate-cathode voltage and conduction delay time by increasing the rise rate of the trigger voltage. However, in the currently adopted series resonance network design schemes, usually the value of inductance is very large, which can easily lead to the decline in the electromagnetic compatibility performance; moreover, the large distribution of network component parameters will greatly increase the fabrication difficulties. In view of the features of high-power hydrogen thyratron and the design requirements of PFN, this paper adopted the series resonance network design scheme to devise network series and parameters of the PFN and analyze the shortcomings of the series resonance network design scheme; then, it used the anti-resonance network to design a three-stage transform algorithm model, so as to achieve the purpose of reducing the inductance of the PFN and the difficulty of capacitance model selection in engineering practice. At last, simulation results verified the correctness and feasibility of the designed three-stage transform algorithm model, providing evidences for the pulse network projects of hydrogen thyratron and other high-power equipment in terms of implementation paths, methods, and algorithm models.

Keywords: anti-resonance; hydrogen thyratron; series resonance; simulation; three-series conversion algorithm model

1 INTRODUCTION

Pulse Forming Network is a widely used field of high power pulse technology. The hydrogen thyratron as power switching in Pulse Forming Network can undertake high power energy. By means of Series resonance network, the order and parameter in Pulse Forming Network can be determined. But the value of inductance and the other components value in Pulse Forming Network which used hydrogen thyratron designed by Series resonance network are so large that it increases the difficulty of manufacturing and cannot be widely used in engineering practice [1-5]. World field scholars have conducted a lot of research on PFN design, for instance, Harchandani and Gorade [6] studied the PFN of Marx generator with boosting operation; scholar Zhu [7] of Xi'an Jiaotong University optimized the design of compact-style PFN; Ma and Li [8] of China Academy of Engineering Physics designed a charging source for PFN formed by cascaded Blumlein pulse; Long and Liu [9] of the National University of Defense Science and Technology of China researched the Marx PFN; Chang [10] of China Academy of Engineering Physics developed a 100 KV low-impedance Blumlein PFN with non-uniformly distributed parameters [11, 12]. In this article, a method is proposed by means of Series resonance network and anti-resonance network, the value of inductance and the other components values are easy to manufacture. Provided is an effective implementation path and equivalent algorithm model for designing the Pulse Forming Network of hydrogen thyratron and other high-power devices.

2 DESIGN PRINCIPLES FOR HYDROGEN THYRATRON-TRIGGERED PFN

This paper took Model CX1159 Hydrogen thyratron as the design object, and the design parameters of the PFN are listed in Tab. 1.

Table 1 Design parameters and requirements of PFN triggered by CX1159 hydrogen thyratron

No.	Name	Requirement
1	Rise rate of triggered forward voltage	≥ 1 KV/μS
2	Top width of backward voltage	> 4 μS

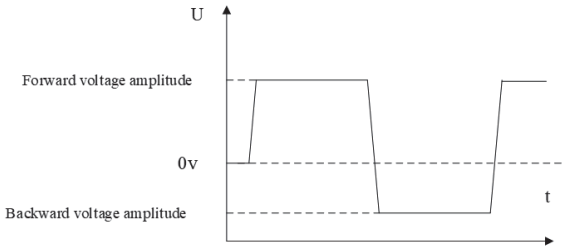

Figure 1 Gate waveform

Hydrogen thyratron-triggered pulse that meets the load pulse requirements consists of a positive trapezoidal pulse (main pulse) and a negative pulse, as shown in Fig. 1. The duty cycle is 50%, the period is 13.6 μs, the duration of positive trapezoidal pulse is 6.8 μs. The main pulse is a trapezoid shaped pulse. Viewing from the perspective of the Fourier series, it can be synthesized by multiple single harmonic waves to meet different waveform design requirements, as shown in Fig. 2.

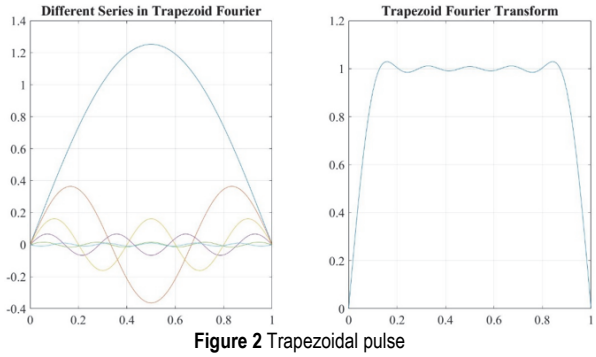

Figure 2 Trapezoidal pulse

When the hydrogen thyratron is idealized as a switch SW, the equivalent circuit of the simplified load circuit model is shown in Fig. 3. The mathematical model of Fig. 4 is:

$$\begin{cases} \dot{V}(x) = V_0^+ \left(e^{-j\beta x} + \Gamma e^{j\beta x} \right) \\ \dot{I}(x) = \dfrac{V_0^+}{\rho} \left(e^{-j\beta x} - \Gamma e^{j\beta x} \right) \end{cases}$$

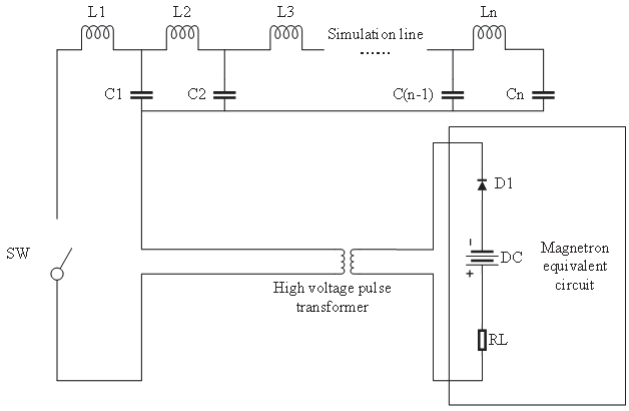

Figure 3 Equivalent circuit of the discharge circuit of pulse modulator

And the load discharge voltage waveform is shown in Fig. 4.

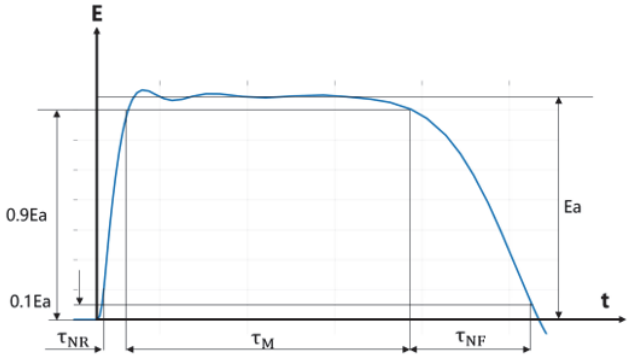

Figure 4 Discharge waveform of load circuit

The load pulse width in Fig. 4 is:

$$\tau_N = \tau_{NR} + \tau_M + \tau_{NF}$$

where, τ_{NR} represents the rise time of the discharge voltage of simulation line; τ_M represents the output pulse width required by the magnetron; τ_{NF} represents the fall time of the discharge voltage of simulation line; then the rise time and fall time are:

$$\tau_{NR} = \tau_{NF} = 0.4\frac{\tau_N}{N}$$

According to the load pulse width requirement, the second gate pulse width of the hydrogen thyratron is:

$$\tau_{g2} = \tau_{g2R} + \tau_N + \tau_{g2F}$$

where, τ_{g2R} represents the trigger voltage rise time of the second gate of the hydrogen thyratron; τ_{g2F} represents the trigger voltage fall time of the second gate of the hydrogen thyratron.

$$\tau_{g2R} = \tau_{g2F} = \frac{\text{Second gate voltage amplitude}}{\text{Second gate voltage rise rate}}$$

The waveform parameters are shown in Fig. 5:

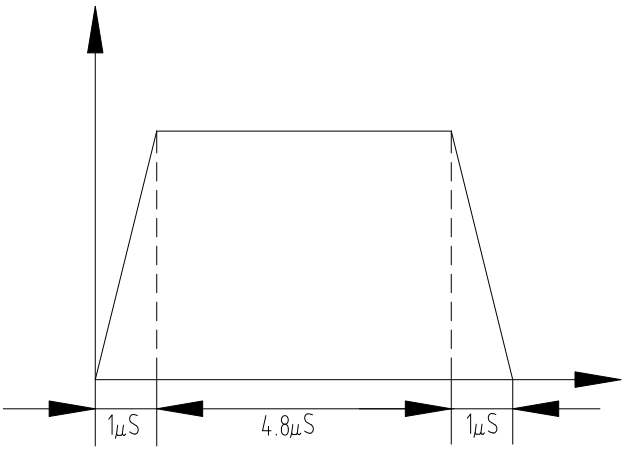

Figure 5 Second gate main pulse

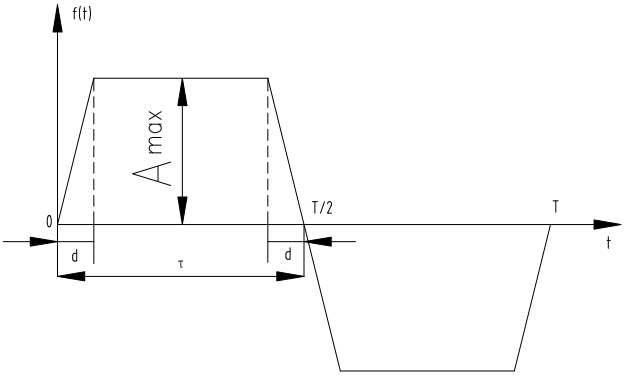

Figure 6 Trapezoidal pulse

The general expression for the Fourier series and coefficients of the trapezoidal pulse with alternating flat top (as shown in Fig. 6) is:

$$f(t) = \frac{A_{\max}}{\pi\omega d}\sum_{n=1}^{+\infty} b_n \sin\left[(2n-1)\omega t\right]$$

where, $b_n = \frac{4\sin\left[(2n-1)\omega d\right]}{(2n-1)^2} n = 1,2,3...$

Let, $\alpha = \frac{d}{\frac{T}{2}}$, and there are $\omega = \frac{2\pi}{T}$, $T = 2\tau$

After sorting out, there is:

$$f(t) = A_{\max}\sum_{n=1}^{+\infty} b_n \sin\left[(2n-1)\frac{\pi}{\tau}t\right]$$

where, $b_n = \frac{4}{\pi}\cdot\frac{1}{2n-1}\cdot\frac{\sin\left[(2n-1)\pi\alpha\right]}{(2n-1)\pi\alpha} n = 1,2,3...$

or:

$$f(t) = A_{\max}\sum_{n=1}^{+\infty}\frac{4}{\pi}\cdot\frac{1}{2n-1}\cdot\frac{\sin\left[(2n-1)\pi\alpha\right]}{(2n-1)\pi\alpha} \cdot\sin\left[(2n-1)\frac{\pi}{\tau}t\right] \quad (1)$$

When fitted in finite series, the resulting waveform is shown in Fig. 2. As can be seen in Fig. 6, the slope of the trapezoid was roughly similar to the slope of the straight line formed by the first peak vertex of the waveform and the zero point; therefore, this straight-line slope was adopted to replace the slope of the trapezoid.

3 DESIGN OF THE HYDROGEN THYRATRON-TRIGGERED PFN

3.1 Hydrogen Thyratron-Triggered PFN Based on Multi-Stage Series Resonance Network

The *n*-stage series resonance network triggered by hydrogen thyratron can be plotted as shown in Fig. 7.

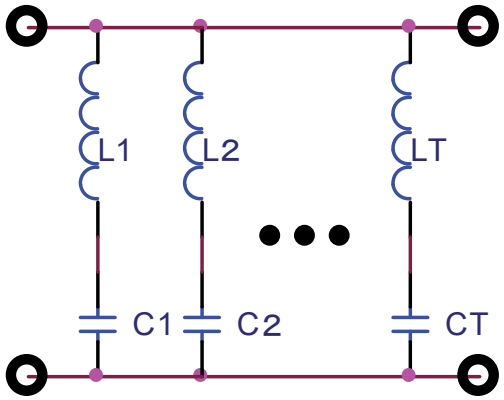

Figure 7 Multi-stage combinatorial resonance network

$$\begin{cases} \text{Expression of the trapezoidal wave: } i_n(t)=\dfrac{E_0}{\rho}\sum_{n=1}^{+\infty}\dfrac{4}{\pi}\cdot\dfrac{1}{2n-1}\cdot\dfrac{\sin\left[(2n-1)\pi\alpha\right]}{(2n-1)\pi\alpha}\cdot\sin\left[(2n-1)\dfrac{\pi}{\tau}\right]t \\ \text{Expression of the circuit network: } i_n(t)=E_0\sum_{n=1}^{+\infty}\sqrt{\dfrac{C_n}{L_n}}\sin\dfrac{t}{\sqrt{L_n\cdot C_n}} \end{cases}$$

where, amplitudes and angles are equal respectively:

$$\begin{cases} \dfrac{E_0}{\rho}\cdot\dfrac{4}{\pi}\cdot\dfrac{1}{2n-1}\cdot\dfrac{\sin\left[(2n-1)\pi\alpha\right]}{(2n-1)\pi\alpha}=E_0\sqrt{\dfrac{C_n}{L_n}} \\ \left[(2n-1)\dfrac{\pi}{\tau}\right]t=\dfrac{t}{\sqrt{L_n\cdot C_n}} \end{cases}$$

Through formula derivation, we can get:

$$\begin{cases} L_n=\dfrac{\rho\tau}{4}\cdot\dfrac{1}{\dfrac{\sin\left[(2n-1)\pi\alpha\right]}{(2n-1)\pi\alpha}} \\ C_n=\dfrac{4}{(2n-1)^2\pi^2}\cdot\dfrac{\tau}{\rho}\cdot\dfrac{\sin\left[(2n-1)\pi\alpha\right]}{(2n-1)\pi\alpha} \end{cases} \tag{3}$$

where, L_n and C_n are respectively the inductance and capacitance in the *n*-th order series resonance circuit of the trapezoidal wave.

They can be expressed as follows as well:

The expression for the series resonance network is:

$$i_n(t)=E_0\sum_{n=1}^{+\infty}\sqrt{\frac{C_n}{L_n}}\sin\frac{t}{\sqrt{L_n\cdot C_n}} \tag{2}$$

When corresponding to the second gate main pulse, Eq. (2) can be expressed as:

$$u_{g2}=E_0\sum_{n=1}^{+\infty}\frac{4}{\pi}\cdot\frac{1}{2n-1}\cdot\frac{\sin\left[(2n-1)\pi\alpha\right]}{(2n-1)\pi\alpha}\cdot\sin\left[(2n-1)\frac{\pi}{\tau}\right]t$$

The current of the second gate main pulse is:

$$i_n(t)=\frac{E_0}{\rho}\sum_{n=1}^{+\infty}\frac{4}{\pi}\cdot\frac{1}{2n-1}\cdot\frac{\sin\left[(2n-1)\pi\alpha\right]}{(2n-1)\pi\alpha}\cdot\sin\left[(2n-1)\frac{\pi}{\tau}\right]t$$

where, ρ represents the characteristic impedance of the circuit. The different current expressions of the hydrogen thyratron-triggered PFN are:

$$\begin{cases} L_n=K_L\cdot\rho\tau \\ C_n=K_C\cdot\dfrac{\tau}{\rho} \end{cases} \tag{4}$$

where, $\begin{cases} K_L=\dfrac{(2n-1)\pi\alpha}{4\sin\left[(2n-1)\pi\alpha\right]} \\ K_C=\dfrac{4}{(2n-1)^3\pi^3}\cdot\dfrac{\sin\left[(2n-1)\pi\alpha\right]}{\alpha} \end{cases}$

For the subsequent circuit of the PFN, the characteristic impedance $\rho=10\ \Omega$, $\tau_{g2}=6.8\ \mu S$, based on these values, the L_n values can be calculated, as shown in Tab. 2.

Table 2 The calculated values of L_n

α	L_1 / μH	L_2 / μH	L_3 / μH	L_4 / μH
0.01	17.00279	17.02517	17.07004	17.13766
0.02	17.01118	17.10099	17.2826	17.56014
0.03	17.02517	17.2284	17.64521	18.29745
0.04	17.04478	17.40904	18.17106	19.40514
0.05	17.07004	17.64521	18.8802	20.97438
0.06	17.10099	17.94002	19.80127	23.15078
0.07	17.13766	18.29745	20.97438	26.16976

Table 2 The calculated values of L_n (continuation)

α	L_1 / μH	L_2 / μH	L_3 / μH	L_4 / μH
0.08	17.18011	18.72248	22.45547	30.42667
0.09	17.2284	19.22124	24.32319	36.62724
0.1	17.2826	19.80127	26.69001	46.14956
0.11	17.34278	20.47173	29.72085	62.06684
0.12	17.40904	21.24383	33.66579	92.84909
0.13	17.48145	22.13124	38.92084	173.2483
0.14	17.56014	23.15078	46.14956	812.9587
0.15	17.64521	24.32319	56.55053	–362.114
0.16	17.73678	25.6743	72.52526	–163.141
0.17	17.83501	27.23655	99.67788	–113.328
0.18	17.94002	29.05116	154.7845	–92.4401
0.19	18.05198	31.17114	321.1006	–82.5853
0.2	18.17106	33.66579	33516.4	–78.635

The values of C_n ($\rho = 10\ \Omega$ $\tau_{g2} = 6.8$ μS) are shown in Tab. 3.

Table 3 The calculated values of C_n

α	C_1 / μF	C_2 / μF	C_3 / μF	C_4 / μF
0.01	0.275828	0.030607	0.01099	0.005585
0.02	0.275692	0.030472	0.010854	0.00545
0.03	0.275465	0.030246	0.010631	0.005231
0.04	0.275148	0.029932	0.010324	0.004932
0.05	0.274741	0.029532	0.009936	0.004563
0.06	0.274244	0.029046	0.009474	0.004134
0.07	0.273657	0.028479	0.008944	0.003657
0.08	0.272981	0.027833	0.008354	0.003146
0.09	0.272216	0.02711	0.007713	0.002613
0.1	0.271362	0.026316	0.007029	0.002074
0.11	0.270421	0.025454	0.006312	0.001542
0.12	0.269391	0.024529	0.005572	0.001031
0.13	0.268276	0.023546	0.00482	0.000552
0.14	0.267073	0.022509	0.004065	0.000118
0.15	0.265786	0.021424	0.003317	–0.00026
0.16	0.264414	0.020296	0.002587	–0.00059
0.17	0.262957	0.019132	0.001882	–0.00084
0.18	0.261418	0.017937	0.001212	–0.00104
0.19	0.259797	0.016717	0.000584	–0.00116
0.2	0.258094	0.015478	5.6E-06	–0.00122

Table 4 Parameter values of the 3-stage series resonance network

L_1 / μH	L_2 / μH	L_3 / μH	C_1 / μF	C_2 / μF	C_3 / μF
17	20	27	0.27	0.026	0.007

As can be seen from the data in the table, there are situations that the inductance tends to infinity and the capacitance tends to zero, or the inductance and capacitance are even negative, which cannot be realized in engineering practice. Theoretically, feasible does not mean practically achievable, and this is the reason why the 4-order fitting of $\alpha = 0.15$ cannot be realized. To achieve a rising slope as accurate as possible, according to the relative slope table, the 3-stage structure of $\alpha = 0.10$ can be adopted to fit the trapezoidal pulse, and the values of L and C are shown in Tab. 4.

After the 3-stage series resonance network structure had been added into the trigger circuit, the simplified circuit and the simulation waveform are shown in Fig. 8.

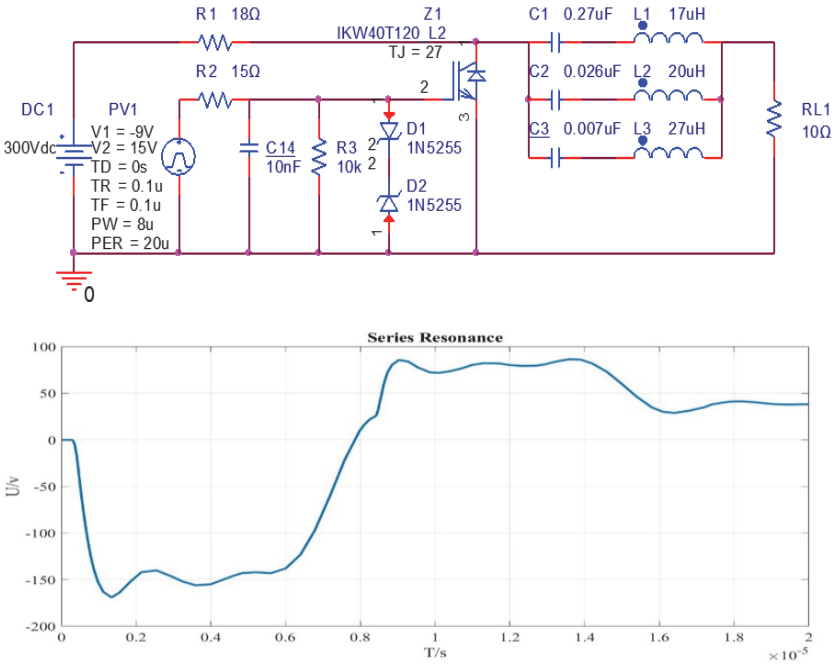

Figure 8 Simplified circuit and simulation waveform of 3-stage series resonance network

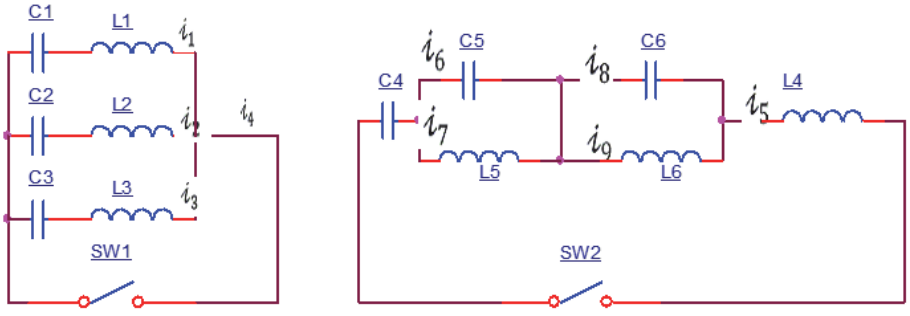

Figure 9 Series resonance network and anti-resonance network

Simulation results showed that the rise time was about 1 μS, through the voltage boost of the pulse transformer, the rise rate reached 1 KV/μS, which met the requirement of the rise rate; the top width of the backward voltage was 5 μS, which met the requirement of not less than 4 μS; and the half-cycle was 7.5 μS. Compared with the design values, the errors of forward amplitude, backward amplitude, rise time, and top width were very small, which met the design requirements. The error of the half-cycle was a bit larger, but it will not affect the pulse operation process.

The series resonance network is based on the Fourier series analysis. This circuit has three obvious defects in engineering practice: first, the large inductance is not conducive to the design of electromagnetic compatibility; second, the inductor fabrication is prone to distributed capacitance, which can damage the pulse waveform; third, the large changes in capacitance value can cause model selection difficulty. Therefore, this paper attempted to use the anti-resonance network to overcome these defects.

3.2 The Hydrogen Thyratron-Triggered PFN Based on Anti-Resonance Network Circuit

When designing the hydrogen thyratron-triggered PFN using anti-resonance network, the anti-resonance is the equivalent exchange of the series resonance network (Fig. 9).

The series resonance network can be written as:

$$i_C(t) = E_0 \sum_{n=1}^{+\infty} \sqrt{\frac{C_n}{L_n}} \sin \frac{t}{\sqrt{L_n \cdot C_n}}$$

Dividing both sides by E_0, we can get:

$$Y_C(t) = \sum_{n=1}^{+\infty} \sqrt{\frac{C_n}{L_n}} \sin \frac{t}{\sqrt{L_n \cdot C_n}}$$

where: $\omega_n = \dfrac{1}{\sqrt{L_n \cdot C_n}}$, $Y(t)$ was subject to Laplace transform to get:

$$Y_C(S) = \sum_{n=1}^{+\infty} \cdot \frac{C_n}{L_n \cdot C_n S^2 + 1}$$

Choose the 3-stage network:

$$Y_C(S) = \frac{\begin{array}{c}(C_1C_2C_3(L_2L_3 + L_1L_3 + L_1L_2)S^4 \\ + \left[\begin{array}{c}(C_1L_2C_2 + C_1L_3C_3) + (L_1C_1C_2 + C_2L_3C_3) \\ + (L_1C_1C_3 + L_2C_2C_3)\end{array}\right] S^2 + (C_1 + C_2 + C_3)\end{array}}{\begin{array}{c}L_1C_1L_2C_2L_3C_3S^6 + (C_1L_1C_2L_2 + C_1L_1C_3L_3 + C_2L_2C_3L_3)S^4 \\ + (L_1C_1 + L_2C_2 + L_3C_3)S^2 + 1\end{array}} \quad (5)$$

The Laplace transform of the anti-resonance network is:

$$\begin{cases} \dfrac{1}{S}\left(E_0 + \dfrac{1}{C_4} I_5(S)\right) + S\left(L_4 I_5(S) + L_5 I_7(S) + L_6 I_9(S)\right) = 0 \\ I_5(S) = I_6(S) + I_7(S) \\ I_5(S) = I_8(S) + I_9(S) \\ SL_5 I_7(S) = \dfrac{1}{SC_5} I_6(S) \\ SL_6 I_9(S) = \dfrac{1}{SC_6} I_8(S) \end{cases}$$

Then we can get:

$$Y_B(S) = \frac{I_5(S)}{-E_0} = \frac{\begin{array}{c}S^4C_4L_5C_5L_6C_6 + S^2C_4(L_5C_5 + L_6C_6) + C_4 \\ S^6(L_4C_4L_5C_5L_6C_6) + S^4(L_4C_4L_5C_5 + L_4C_4L_6C_6 + L_5C_5L_6C_6 + C_4L_5L_6C_6 + C_4L_5C_5L_6) \\ + S^2(L_4C_4 + L_5C_5 + L_6C_6 + C_4L_5 + C_4L_6) + 1\end{array}} \quad (6)$$

Eqs. (5) and (6) are equivalent, and there is:

$$\begin{cases} C_4L_5C_5L_6C_6 = C_1C_2C_3(L_2L_3 + L_1L_3 + L_1L_2) \\ C_4(L_5C_5 + L_6C_6) = (C_1L_2C_2 + C_1L_3C_3) + (L_1C_1C_2 + C_2L_3C_3) + (L_1C_1C_3 + L_2C_2C_3) \\ C_4 = C_1 + C_2 + C_3 \\ L_4C_4L_5C_5L_6C_6 = L_1C_1L_2C_2L_3C_3 \\ L_4C_4L_5C_5 + L_4C_4L_6C_6 + L_5C_5L_6C_6 + C_4L_5L_6C_6 + C_4L_5C_5C_6 \\ \quad = C_1L_1C_2L_2 + C_1L_1C_3L_3 + C_2L_2C_3L_3 \\ L_4C_4 + L_5C_5 + L_6C_6 + C_4L_5 + C_4L_6 = L_1C_1 + L_2C_2 + L_3C_3 \end{cases} \quad (7)$$

This transform equation is applicable to the mutual transformation between series resonance network and anti-resonance network, since it is independent of the waveform, it can adapt to the parameter conversion of all waveforms. The series resonance data (the values of L and C when $\alpha = 0.1$) were input into Eq. (7) to calculate the anti-resonance parameters, as shown in Tab. 5.

The simulation results showed that the rise time of the anti-resonance network was about 1 μS, through the voltage boost of the pulse transformer, the rise rate reached

1 KV/μS; the top width of the backward voltage was 5 μS, which met the requirement of not less than 4 μS; and the half-cycle was 7.5 μS. Compared with the design values, the errors of forward amplitude, backward amplitude, rise time, and top width were very small, which met the design requirements. Compared with the series resonance network (Fig. 11), simulation waveforms' forward amplitude is 165 v. backward amplitude is 75 v. rise time is 1 μs top width is 5 μs. Two waveforms coincide and satisfied the electric circuit requirement. The simulation proves Series resonance network and anti-resonance network equivalent.

Table 5 Series resonance network and anti-resonance network parameters

Series resonance parameters	L_1/ μH	L_2/ μH	L_3/ μH	C_1/ μF	C_2/ μF	C_3/ μF
	17	20	27	0.27	0.026	0.007
Calculated values of anti-resonance	L_4/ μH	L_5/ μH	L_6/ μH	C_4/ μF	C_5/ μF	C_6/ μF
	6.86	5.65	1.16	0.3	0.16	0.2

Comparison of the parameters of these two types of circuit showed that the inductance of the anti-resonance network was significantly lower than that of the series resonance network, its electromagnetic compatibility was better. During industrial application, the value of distributed capacitance can be reduced, so that the actual product waveform is closer to the theoretical value, and the waveform is better; in anti-resonance network, the distribution of the capacitance is concentrated, the model selection of capacitor is easier, so it is more convenient to be applied in the engineering practice; while for the series resonance network, there is a large difference in the capacitance value, and it is harder to be applied in the engineering practice. In summary, the conversion algorithm realizes the parameter exchange of series resonance and anti-resonance networks. The simulated waveform comparison result shows that the output waveforms before and after the conversion meet the design requirements. The correctness of the conversion algorithm is verified, and the circuit parameters are easier to implement in the engineering. The conversion algorithm has great engineering utility value.

The anti-resonance network and simulation waveform are (Fig. 10):

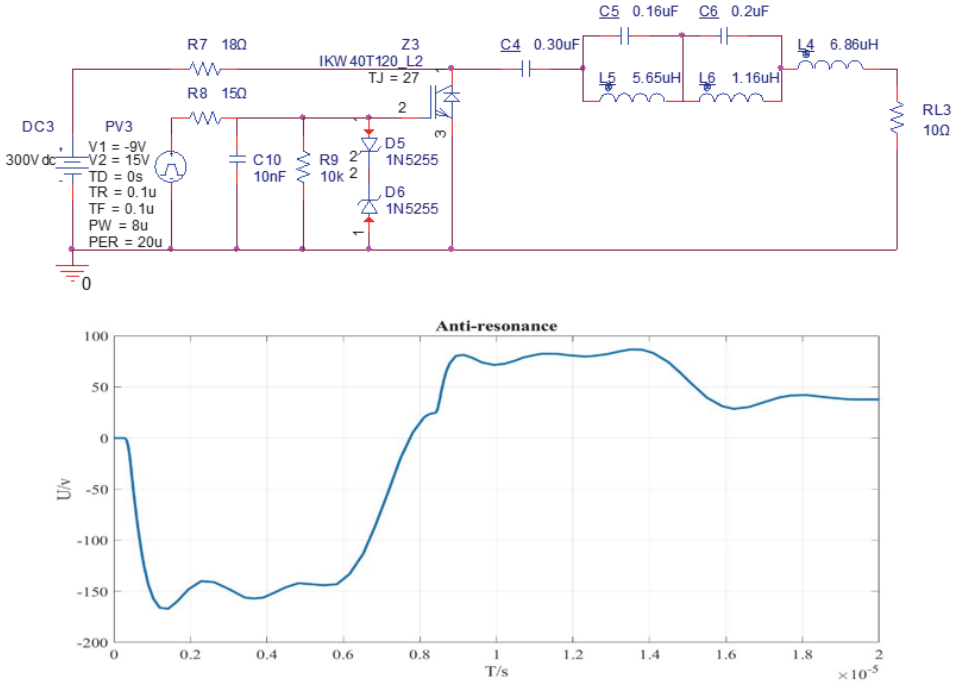

Figure 10 The anti-resonance network and simulation waveform

Comparison of simulation graphs:

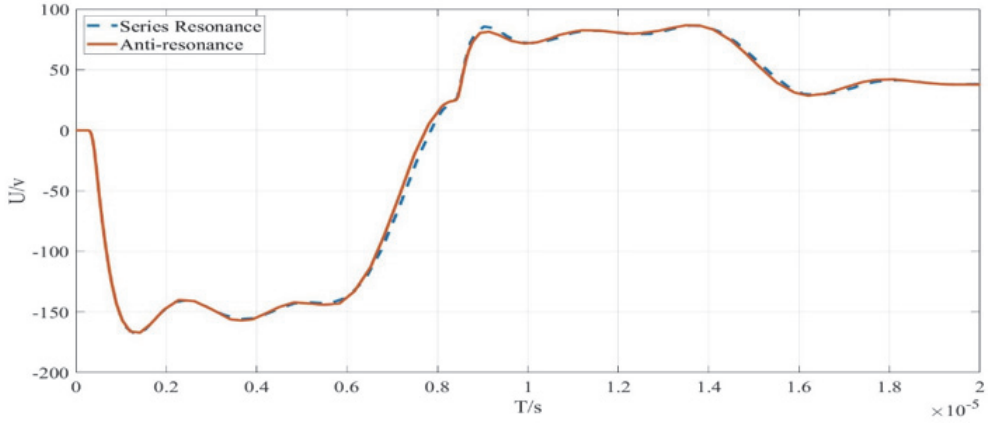

Figure 11 Comparison of simulation waveforms of series resonance network and anti-resonance network

4 OPTIMIZATION AND EFFECT VERIFICATION OF THE WAVEFORM OF PFN

The capacitance and inductance of the designed hydrogen thyratron-triggered PFN were optimized and verified by directly fitting the trapezoidal pulse with Fourier series to make the top flatter.

Fourier Series: $f(t) = A_{\max} \sum_{n=1}^{+\infty} b_n \sin\left[(2n-1)\omega t\right]$.

Set $A_{\max} = 1$, if the series is 2, then there is:

$$f(t) = b_1 \sin \omega t + b_2 \sin 3\omega t$$

Let $b_1 = 1$, by changing b_2, the following wave family could be plotted, as shown in Fig. 12:

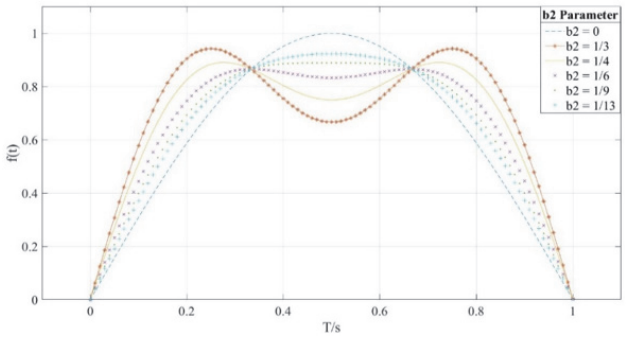

Figure 12 The waveform family of b_2

By observing the waveform family, we can know that:

(1) The waveform family has 2 intersection points, and the intersection time of the two intersection points will not change with parameter b_2;

(2) The value of b_2 determines the height of the vertex (top flatness);

(3) When the top is flat, the value of b_2 coefficient is unique.

When the top is flat, the values of the vertex and the intersection points of the wave family should be the same:

$$b_1 \sin \omega \frac{T}{6} + b_2 \sin 3\omega \frac{T}{6} = b_1 \sin \omega \frac{T}{4} + b_2 \sin 3\omega \frac{T}{4}$$

Let $b_1 = 1$, it could be solved that $b_2 = \frac{1}{7.46}$.

Based on the same principle, for the series of 3, there is: $f(t) = b_1 \sin \omega t + b_2 \sin 3\omega t + b_3 \sin 5\omega t$.

Let $b_1 = 1$, b_2 takes step values, then by changing b_3, the following wave family could be plotted, as shown in Fig. 13:

By observing the waveform family, we can know that:

(1) The wave family has 4 intersection points, and the intersection time of all intersection points will not change with parameters b_2 and b_3;

(2) The value of b_2 determines the height of the two intersection points in the middle;

(3) The value of b_3 determines the height of the vertex (single point);

(4) The values of b_2 and b_3 coefficients are unique.

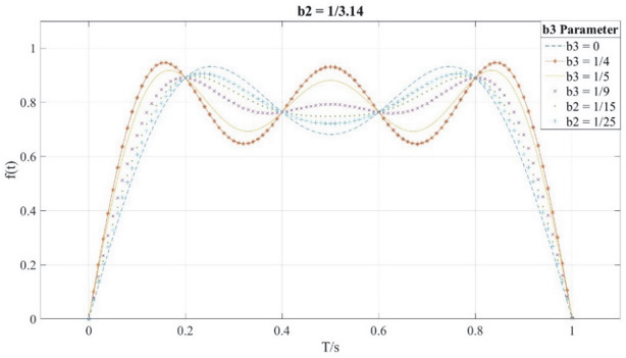

(a) $b_2 = \frac{1}{3.14}$

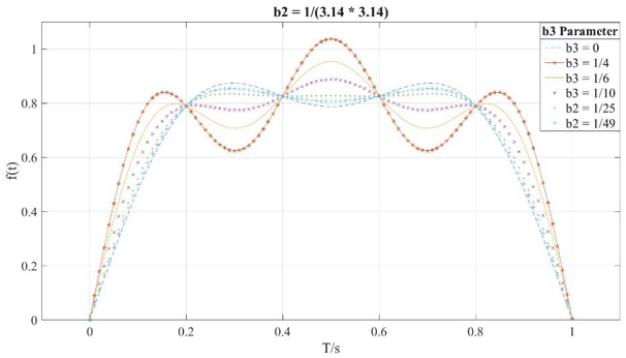

(b) $b_2 = \frac{1}{1.5 \times 3.14}$

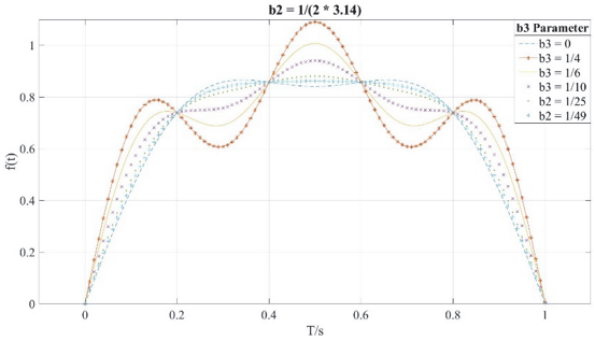

(c) $b_2 = \frac{1}{2 \times 3.14}$

Figure 13 The waveform family of b_3

After subjected to simulation experiments, it is found that when the coefficients $\frac{1}{b_1} : \frac{1}{b_2} : \frac{1}{b_3} = \frac{1}{1} : \frac{1}{5} : \frac{1}{25}$, the waveform is flat. For the 3-series Fourier series of the trapezoidal pulse, there is:

$$b_n = \frac{4}{\rho\pi} \cdot \frac{1}{2n-1} \cdot \frac{\sin\left[(2n-1)\pi\alpha\right]}{(2n-1)\pi\alpha} \quad n = 1,2,3...$$

With the first series as the benchmark, the b_1 of first series was calculated when $\alpha = 0.1$, and $\rho = 10\ \Omega$:

$$b_1 = \frac{4}{\rho\pi} \cdot \frac{1}{1} \cdot \frac{\sin(\pi \times 0.1)}{\pi \times 0.1} = \frac{4}{10 \times 3.14} \cdot \frac{0.308866}{3.14 \times 0.1} = 0.1253$$

$$\text{If } \omega = \frac{\pi}{\tau} = \frac{\pi}{6.8 \times 10^{-6}} = 4.6 \times 10^5$$

$$f(t)=0.1253\sin 4.6\times10^{5}t+0.02506\sin 1.38\times10^{6}t$$
$$+0.005012\sin 2.3\times10^{6}t$$

When corresponding to the series resonance network, the expression is:

$$i_t(t)=E_0\sum_{n=1}^{+\infty}\sqrt{\frac{C_n}{L_n}}\sin\frac{t}{\sqrt{L_n\cdot C_n}}$$

It can be calculated that:

$$\begin{cases}\sqrt{\dfrac{C_1}{L_1}}=0.1253\\ \dfrac{1}{\sqrt{L_1\cdot C_1}}=4.6\times10^{5}\end{cases}\quad\begin{cases}\sqrt{\dfrac{C_2}{L_2}}=0.02506\\ \dfrac{1}{\sqrt{L_2\cdot C_2}}=1.38\times10^{6}\end{cases}$$
$$\begin{cases}\sqrt{\dfrac{C_3}{L_3}}=0.005012\\ \dfrac{1}{\sqrt{L_3\cdot C_3}}=2.3\times10^{6}\end{cases}$$

After optimization, the solved parameters of the series resonance network are shown in Tab. 6.

The circuit level simulation is shown in Fig. 14:

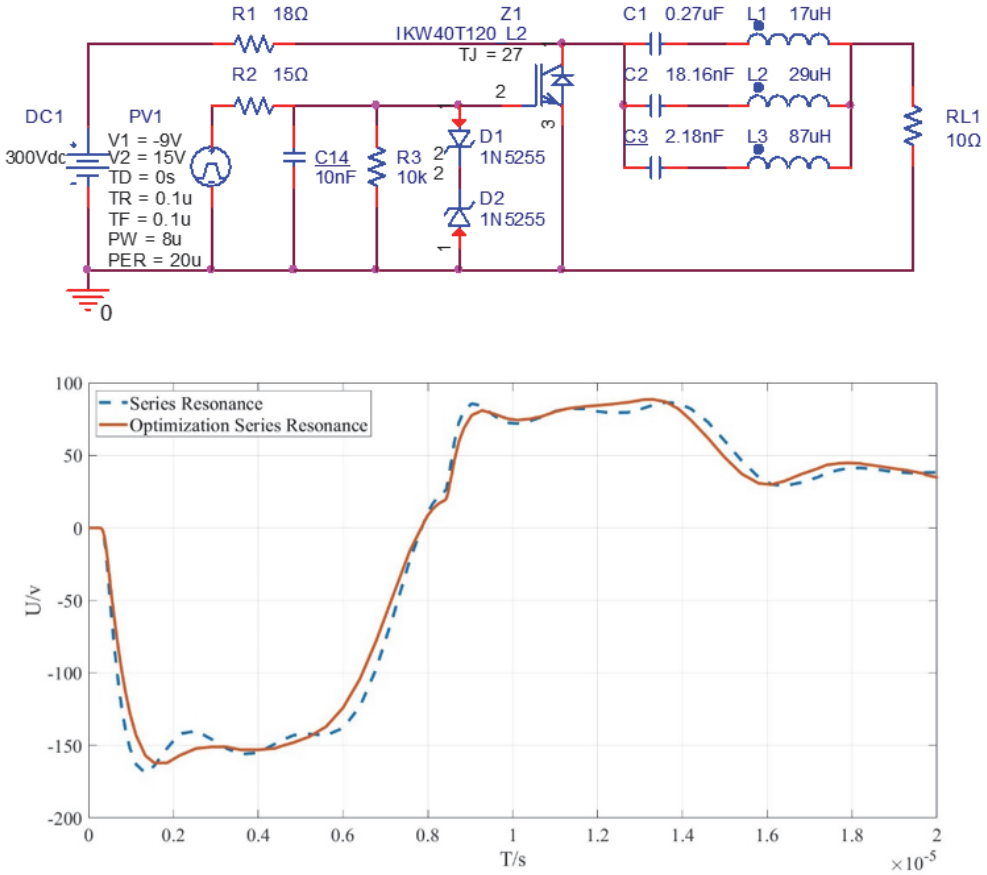

Figure 14 Comparison of series resonance waveforms before and after 3-stage optimization

Table 6 Optimized parameters of series resonance network

L_1 / μH	L_2 / μH	L_3 / μH	C_1 / μF	C_2 / nF	C_3 / nF
17	29	87	0.27	18.16	2.18

The simulation results showed that the waveform rise time before optimization was 0.5 S, the waveform rise time after optimization was 0.7 S. As the parameters are shown in Tab. 4 and Tab. 6, the inductance and capacitance values are changed except for the first stage inductance value of 27 μH which remained unchanged. Simulation results show that the parameter-optimized waveform rise time does not meet the waveform setting requirements, but the waveform becomes flatter. Although the optimization had improved the waveform flatness, it ignored other analysis methods, which had resulted in changes in the rise time, and such changes are not expected in the engineering practice. If the loss of rise time is acceptable, then this parameter can be used to optimize the series resonance network and the anti-resonance network, but the proposed pulse network design needs to consider both the rise rate and the flatness, so the method after optimization was not adopted.

5 CONCLUSION

This paper aims to optimize the design method about parameters of the hydrogen thyratron pulse formation network. Three order series resonance pulse formation network expressions are presented. On this basis, we also derive the equivalent algorithm model analytical expression for the 3-order series resonance and anti-resonance pulse network. And the individual component parameters are also calculated. A design method based on

order 3 series resonance and reverse resonance pulse formation network equivalent conversion is proposed. The proposed method can be used to design special networks that qualify the network elements. Simulation results show that the proposed equivalent algorithm model is correct. The equivalent calculation of the parameters of series resonance and anti-resonance network components is feasible. This equivalent algorithm model can effectively reduce the inductance value and the distribution of component values in the network. It provides a feasible scheme for the pulse source design of hydrogen thyratron and other high-power devices. The next step will be the physical verification of the parameters which are designed by the proposed method.

Acknowledgments

This work was sponsored by Artificial Intelligence Key Laboratory of Sichuan Province (No.: 2021RYY01) and the Science and Technology Plan Project of Sichuan Province under contract (No.: 2021YJ0058).

6 REFERENCES

[1] Wang, C. & Li, H. (2020). Design of trapezoidal pulse forming network based on simplex optimization method. *Intense Laser and Particle Beams*, *32*(6), 118-124.

[2] Wang, C. & Li, H. (2018). Theoretical analysis and design of quasi-square wave pulse formation network. *Strong Laser and Particle Beam*, *30*(3), 114-119.

[3] Zhu, F. & Xiong, C. Z. (2017). Characteristics of wide flat top pulse formation network discharge. *Internet of Things Technology*, *7*(5), 46-49.

[4] Hosseini, S. M. H., Ghafourinam, H. R., & Oshtaghi, M. H. (2018). Modeling and construction of Marx impulse generator based on boost converter pulse-forming network. *IEEE Transactions on Plasma Science*, *46*(10), 3257-3264. https://doi.org/10.1109/TPS.2018.2864333

[5] Nagaraju, S., Ramaswamy, N. K., & Ramaswamy, R. K. (2023). Design and Implementation of Hybrid Controller for Dynamic Power Management in a DC Microgrid. *Journal of Intelligent Systems and Control*, *2*(1), 1-12. https://doi.org/10.56578/jisc020101

[6] Harchandani, R. & Gorade, P. (2017). Pulse forming network for Marx generator with boosting operation. *2017 2nd IEEE International Conference on Recent Trends in Electronics, Information & Communication Technology (RTEICT)*, 1768-1771. https://doi.org/10.1109/RTEICT.2017.8256903

[7] Zhu, Y. (2016). Optimization design of compact pulse forming network. *Strong Laser and Particle Beam*, *9*, 274-276.

[8] Ma, X. & Li, H. (2013). Cascade Blumlein pulse forming network charging power supply design. *Electronics Design Engineering*, *21*(3), 157-159.

[9] Long, X. F. & Liu, Y. (2008). Research on Marx pulse forming network. *Chinese Physics*, *32*, 274-276.

[10] Chang, A. (1997). Development of a 100kV low impedance nonuniform concentration parameter Blumlein pulse forming network. *Intense Laser and Particle Beam*, *9*(3), 331-335.

[11] Nunnally, W. C. (2005). Critical component requirements for compact pulse power system architectures. *IEEE Transactions on Plasma Science*, *33*(4), 1262-1267. https://doi.org/10.1109/TPS.2005.852406

[12] Zheng, X., Li, W., & Pan, H. (2006). Radar Launch Technology. *Beijing: Electronics Industry Press*, *231*, 1-1.

Contact information:

Yong HAN
Intelligent manufacturing and automotive College,
Chengdu Vocational & Technical College of Industry,
Chengdu 610218, China
E-mail: 35824698@qq.com

Tao ZHAO
Intelligent manufacturing and automotive College,
Chengdu Vocational & Technical College of Industry,
Chengdu 610218, China
E-mail: tiane_z@hotmail.com

Shi YAN
Academic Research Department,
Chengdu Vocational & Technical College of Industry,
Chengdu 610218, China
E-mail: 510266833@qq.com

Guang WEN
Intelligent manufacturing and automotive College,
Chengdu Vocational & Technical College of Industry,
Chengdu 610218, China
E-mail: 57438701@qq.com

Zhaoyu WU
(Corresponding author)
Intelligent manufacturing and automotive College,
Chengdu Vocational & Technical College of Industry,
Chengdu 610218, China
E-mail: wuzhaoyu@shu.edu.cn